Observations and modeling of synchronized bursting in two-dimensional neural networks

Ronen Segev,[1] Yoash Shapira,[1] Morris Benveniste,[2] and Eshel Ben-Jacob[1,*]
[1]*School of Physics and Astronomy, Raymond and Beverly Sackler Faculty of Exact Sciences, Tel-Aviv University, Tel-Aviv 69978, Israel*
[2]*Department of Physiology and Pharmacology, Sackler Faculty of Medicine, Tel-Aviv University, Tel-Aviv 69978, Israel*
(Received 1 November 2000; revised manuscript received 6 April 2001; published 27 June 2001)

We present long-term (~hours) measurements of the spontaneous activity of two-dimensional cortical cell neural networks placed on multielectrode arrays. We compare histograms of single neuron interspike intervals and the network intersynchronized bursting events intervals. In addition, the effect of Ca concentration on the network activity is being studied. At 1 mM Ca concentration, the network exhibits periodic synchronized bursting that fades away after about 20 min. We present a feedback-regulated integrate and fire model to account for the observations. In the model we include two additional features: dynamical threshold and synapse fatigue.

DOI: 10.1103/PhysRevE.64.011920 PACS number(s): 87.17.−d, 05.70.Ln, 82.40.Bj

I. INTRODUCTION AND MOTIVATION

The neural network is the organizational link that allows a collection of individual neurons that can generate action potentials to become a functioning brain. In principle, one would like to study three-dimensional (3D) *in vivo* neural networks. However, it is difficult to visualize them and measure the electrical activity. Hence, much effort has recently been devoted to the study of two-dimensional (2D) *in vitro* neural networks, in which neural activity can be measured by means of a 2D array of microelectrodes, and network morphology is visualized by light microscopy. In addition, control of the chemical environment of the network, which is difficult *in vivo*, is greatly simplified for *in vitro* networks, and the effect of different drugs can be studied [1]. Furthermore, the ability to characterize 2D networks in great detail affords quantitative comparisons between experimental results and network models.

Much effort has been devoted to show that the morphological and electrophysiological developments in 2D neural networks mimic neuronal development *in vivo* [2,3]. For example, *in vitro* neurite outgrowth and branching is most prominent during the first two weeks, and synapse formation starts at about four days, peaks at three weeks and then stabilizes at a lower level between four to six weeks. In addition, quantitative analysis of neuronal spike trains recorded with intracellular glass electrodes has revealed specific development trends in neuronal firing patterns [2,4] which are similar to those observed *in vivo* [5–7].

Here we present studies of such 2D neural networks. The networks are composed of about 10^6 cells, both neurons and glia. The cells are grown on arrays of 60 microelectrodes. The neurons are randomly attached to the surface. Not all 60 electrodes have neurons attached to them, while some electrodes can have more than one neuron attached. The capacitance coupling between the neurons' membrane and the electrode allows recording of the spontaneous electrical activity [8,3,2,9–12]. The electrodes are 30 μm in diameter and 200 μm apart and arranged in a square array. Our recording area then covered ~1 mm^2 out of the ~3 cm^2 total area of the 2D neural network.

We observed two distinct patterns of activity: (1) periods of sporadic firing of individual neurons and (2) synchronized bursting events in which all the neurons fire several times within a short-time interval (~200 msec) [9]. Similar patterns of activity have been observed in many *in vivo* neuronal tissues [5–7].

We studied the distribution of the intersynchronized bursting event intervals (ISBI) and showed that it is similar to that of single neuron interspike intervals (ISI). It is interesting to note that a similar property has also been found in the beating of heart cells *in vitro* [13]. This might indicate that it is a general property of biological excitatory systems. Next, we studied the internal structure of the synchronized bursting events and showed the existence of early and late phases of neural firing. At the early phase the neurons burst rapidly during a short-time interval (~5 msec), followed by the late phase, which is characterized by a long decay (~200 msec) of neuronal activity.

Experimental observations were then compared with the integrate and fire model [14–16]. While this model can produce synchronized bursting events, the ISBI distribution of this model is finite in short-time intervals unlike the experimental one. Hence, we included in our model two additional experimentally known features: (1) an activity-dependent threshold for the action potential and (2) an activity-dependent synaptic strength. Inclusion of these features into the integrate and fire model produces a model that adequately describes the experimental observations.

The extracellular Ca is known to affect the action potential firing threshold (see [15]) and synapse probability of neurotransmitter release [14,17]. Hence, we studied the effect of Ca^{2+} concentration on the synchronized bursting events in order to reveal the Ca effect on the network behavior. Using 1 mM Ca^{2+}, we observed that neuronal activity is almost periodic and the network has short (~1 sec) ISBI. At lower (0.5 Mm) and higher (2 mM) Ca levels we observed aperiodic synchronized bursting. Using our version of the integrate and fire model, we show that by adjusting the maximum synaptic efficacies we can reproduce these ob-

*Corresponding author. FAX: 972-3-6422979. Email address: eshel@venus.tau.ac.il

served phenomena. We also found that after ~20 min in the presence of 1 mM Ca^{2+}, the periodic activity of the network fades away. Afterwards, the network exhibits aperiodic activity without any significant change for ~20 h. We conclude that the network demonstrates an interesting adaptive capability to the imposed external conditions. At present we do not know why the periodic activity fades away.

In Sec. II we describe the experimental methods we used to culture and measure the network activity. In Sec. III we describe the experimental observations. In Sec. IV we present the new regulated feedback model and discuss the biophysical basis of the observed activity. Finally, we discuss the theoretical and experimental results in Sec. V.

II. EXPERIMENTAL METHODS

A. Cell culture

Dissociated cortical cultures were prepared and maintained as follows: the entire cortices from one-day-old Charles River rats were finely chopped. The cortical tissue was digested with 0.065% trypsin (Biological Industries, Beit Ha-Emek, catalog 03-046-1b) in phosphate buffered saline (Biological Industries, catalog No. 02-023-1a), for 15 min, followed by mechanical dissociation by trituration. Cells were resuspended in a modified essential medium with Eagle's salts (Biological Industries, catalog No. 01-025-1a) containing 5% horse serum (Biological Industries, catalog No. 04-001-1a), 1 mg/ml gentamycin, and 0.02 mM glucose, and plated on the multielectrode array which was previously coated with poly-D-lysine (Sigma, catalog No. p-7889). The culture was maintained at 37 °C with 5% Co_2 and 95% humidity for 10 days before measurements began. In this paper we describe results obtained from 18 cell cultures that were obtained from different animals.

B. Measurement conditions

All measurements of the spontaneous activity were made in an extracellular solution containing 160 mM NaCl, 2.5 mM KCl, 10 mM hepes (Sigma, catalog No. h-3375), 10 mM glucose, and 1 ml/500 ml phenol red (Sigma, catalog No. p-0383); pH and osmolarity were adjusted to 7.3 and 325 mosm, respectively. To the basic extracellular solution, $CaCl_2$ was added as stated in the text. Data was recorded at 37 °C. In the long-term experiments we used a 100% humidity chamber to prevent evaporation.

C. Data acquisition

Extracellular recordings were made utilizing a multielectrode array (MEA) consisting of 60 substrate-integrated thin-film microelectrodes (MEA-chip, Multi Channel Systems) [18], of 10 μm width and 200 μm between the electrodes. The electrode impedance is 100–500 kΩ at 1 KHz, and its bandwidth of 10 Hz to 3 kHz permits the recording of individual spikes. Low-noise amplifiers are integrated on a single board (B-MEA-1060, amplifier, gain $\times$2000 with a band-pass filter 200 Hz–5 kHz, Multi Channel Systems). The signals collected from the microelectrodes have been digitized and stored in a personal computer equipped with a 16-channel, 12-bit data acquisition board (Microstar DAP, 770 K samples/sec) and a multiplexer that enables simultaneous 60 electrode recording at a rate of 12 K samples/sec per electrode. The data was acquired using Alpha-Map data acquisition software (Alpha Omega Engineering, Israel).

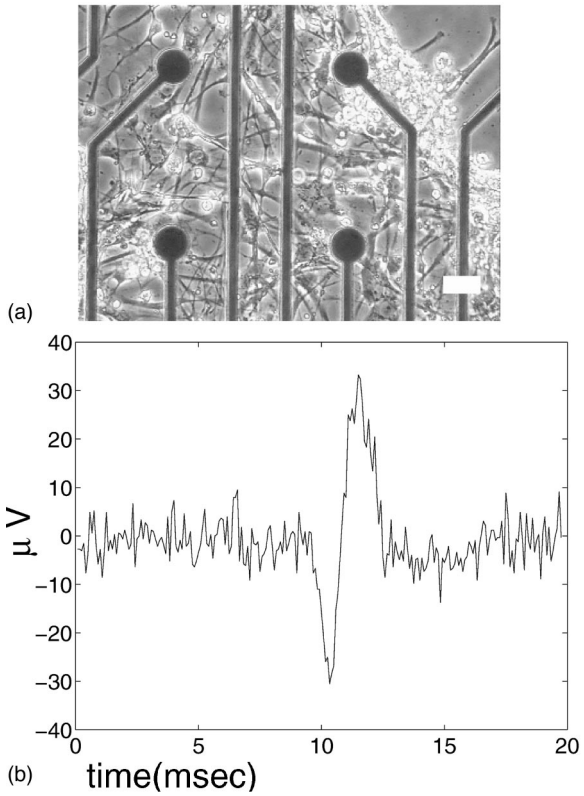

FIG. 1. (a) Neurons on top of an electrode array after 10 days *in vitro*: the electrodes are 30 μm in diameter (error bar=10 μm). The typical cells are ~10 μm in diameter. The thin filaments between the cells are the axon and dendrites. (b) An example of a spike measured by an extracellular electrode. Typically, the neural spike is 2–4 msec in duration as measured from extracellular electrodes.

Data from each electrode array was recorded continuously. All the electrodes that detected spikes were selected for data acquisition and the recorded data was kept on a disk. A threshold detector was used to mark voltage amplitudes which exceeded the noise by 3.5-fold. In a typical experiment there are 10–20 electrodes that detect spikes and ~20% that record more then one neuron. Analysis and sorting of the extracellular recording were made by our method based on wavelet packet decomposition as described in [19].

III. EXPERIMENTAL RESULTS

A. Synchronized bursting events

Characterization of the 2D neural networks experimental system started by measuring the ISI between successive action potentials recorded extracellularly from individual neurons situated on the microelectrodes arrays (Fig. 1). Histograms of the ISI from three different neurons are shown in Fig. 2. The differences in ISI histograms may arise from the

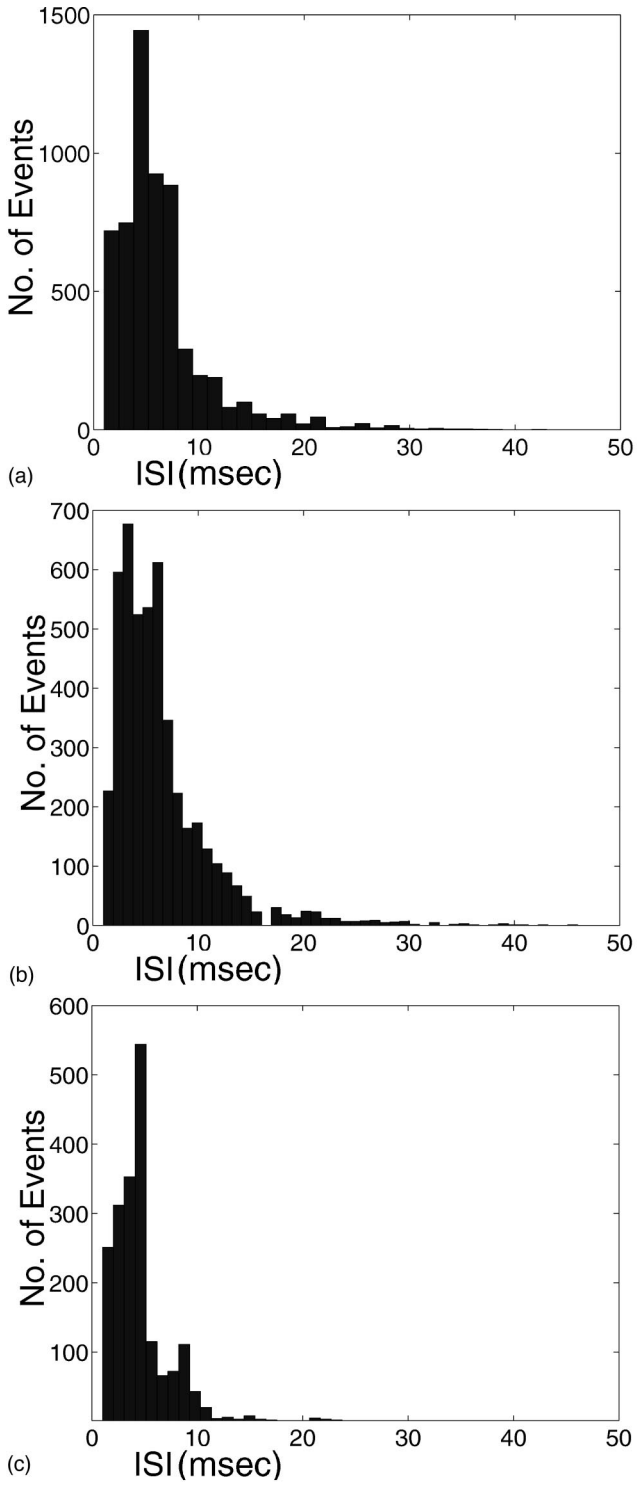

FIG. 2. Three typical examples of the neurons' ISI. There is an absolute refractory period followed by a long decay of neuronal activity. The distribution of the histogram is different due to the intrinsic properties of the neurons or the differences in the wiring of neurons to the network (all neurons are from a single preparation).

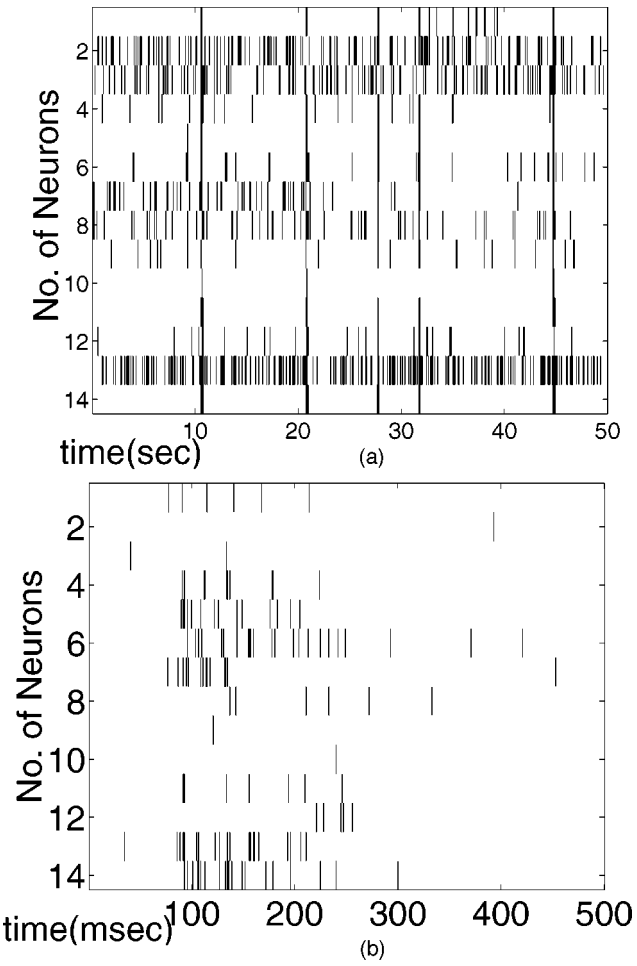

FIG. 3. Spontaneous activity of normal cell culture in a growth medium 30 sec after the CO_2 atmosphere was removed, i.e., the ph was 7.3. (a) Raster plot with 0.1 sec time bins. (b) Zoom into the synchronized bursting events (time bin 1 msec) at the middle of the raster plot in (a) (22 sec).

intrinsic properties of the neurons or the differences in the way the neurons are coupled to the network. Although the action potentials are 2–4 msec in duration, the exact timing of the action potential can be detected in ~ 0.1 msec resolution due to the sharp voltage waveform of the extracellular recording [see the lowest voltage point at Fig. 1(b)]. In all of the examples shown, the neurons have an absolute refractory $\leqslant 2$ msec. The refractory period is followed by a high probability to fire at intervals of about $\sim 8-10$ msec. The histogram has a long tail decay of ~ 70 msec as described before in many systems (see [14] and references therein).

Individual neurons also exhibit two distinct spontaneous firing dynamics: (1) Sporadic neuron firing where the neurons fire randomly one at a time. (2) Synchronized bursting events in which all the neurons spike several times within a short-time interval (~ 200 msec). The detection of these events is done by moving a threshold detector over the raster plot with 100 msec time bins. Then, we detect the time bins in which 80% of the neurons showed at least one spike during that bin. In Fig. 3(a) we show a raster plot of typical activity of a normally developed network after 10 days in culture. The synchronized bursting events are the predominant feature of cortical neural networks in a culture occuring in almost all network conditions as well as in several *in vivo* systems [5–7].

During the synchronized bursting event, each neuron has its own firing pattern. Different neurons fire from 1–2 spikes to ~25 spikes during each event. In Fig. 3(b) we show a zoom in time of the synchronized bursting events. The neurons start to burst within a very-short-time interval (~5 msec) and there is a long (~150 msec) decay of the network activity.

After a synchronized event is triggered, the system enters an absolute refractory period during which there is no synchronized bursting. Note that both the single neuron and the entire network exhibit absolute refractoriness. The typical ISBI is of the order of 5 sec as we show in Fig. 4. Furthermore, the histogram shows long tail decay although ~95% of the probability mass is below 50 sec.

B. The effect of Ca concentration

Keeping in mind the motivation presented in the Introduction, we performed measurements of the network spontaneous dynamics at different levels of Ca^{2+} concentration. The cell cultures were prepared by growing neurons for 10 days. Then the growth medium was replaced by extracellular solution containing different levels of $CaCl_2$. The electrical measurements were performed about 60 sec after the extracellular solution was added.

As expected, the networks show strong dependence on the Ca concentrations. At both 0.5 and 2 mM Ca^{2+} concentrations the activity pattern is aperiodic. The neurons fire randomly, and occasionally there are synchronized bursting events (Figs. 3 and 5). However, intermediate levels of Ca^{2+} concentrations around 1 mM have a dramatic effect: the network's activity turns into almost periodic and rapid (~2 sec) synchronized bursting (see Fig. 5), in agreement with the observations of Maeda *et al.* [9].

C. Long-term behavior

The novelty of our system is the ability to perform long-term recordings (dozens of hours). In Fig. 6 we show the raster plot of the network dynamics at 1 min and 60 min after the 1 mM Ca^{2+} was added. After 1 min, the network shows the almost periodic and rapid (~2 sec) synchronized bursting as described before. However, after 60 min the network activity becomes aperiodic synchronized bursting. To ensure that the observed change in the activity was not due to the deterioration of the network, we continued recording for 15 h after this data was collected and did not notice any significant change in the activity.

Next we studied the transition between periodic and aperiodic network activities. It is natural to use time-dependent Fourier transform methods to analyze the long-term network activity. Our method involves calculating the population total activity at each time bin, then dividing this time sequence into windows. Using the Welch method of power spectrum estimation [20], we calculate the power spectrum of each window. The result is a time sequence of power spectrum estimations. In Fig. 7 we show the development in time of the power spectral density (PSD) of the network activity. The PSD shows at the beginning two high peaks that correspond to the first and second harmonics of the periodic network activity. After about 15 min the PSD becomes flat, and

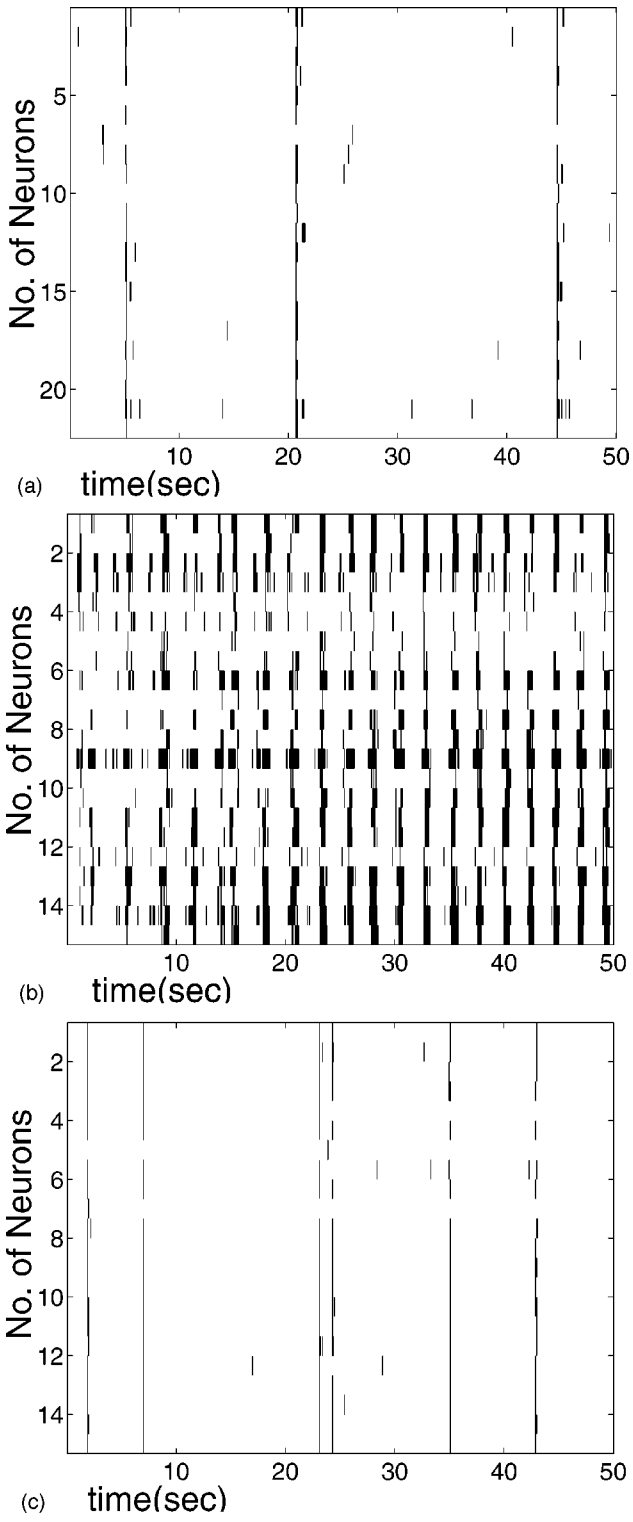

FIG. 4. The effect of Ca concentration on network activity: a raster plot with a 0.1 sec bin. (a) 0.5 mM Ca concentration. (b) 1 mM Ca concentration. (c) 2 mM Ca concentration. The network activity is aperiodic under 0.5 mM Ca and 2 mM Ca and periodic at 1 mM Ca (data are from a single preparation).

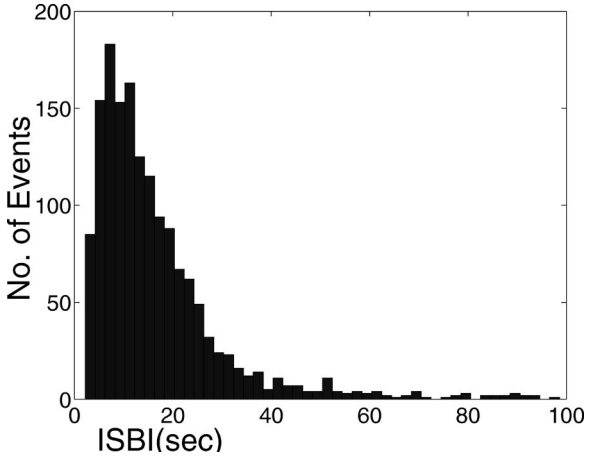

FIG. 5. ISBI calculated from ~15 h recording (0.5 mM Ca concentration).

the periodic activity fades away. An interesting feature of the observed transition is that there is no change in the frequency of the periodic activity during this transition as is seen from the PSD (Fig. 7).

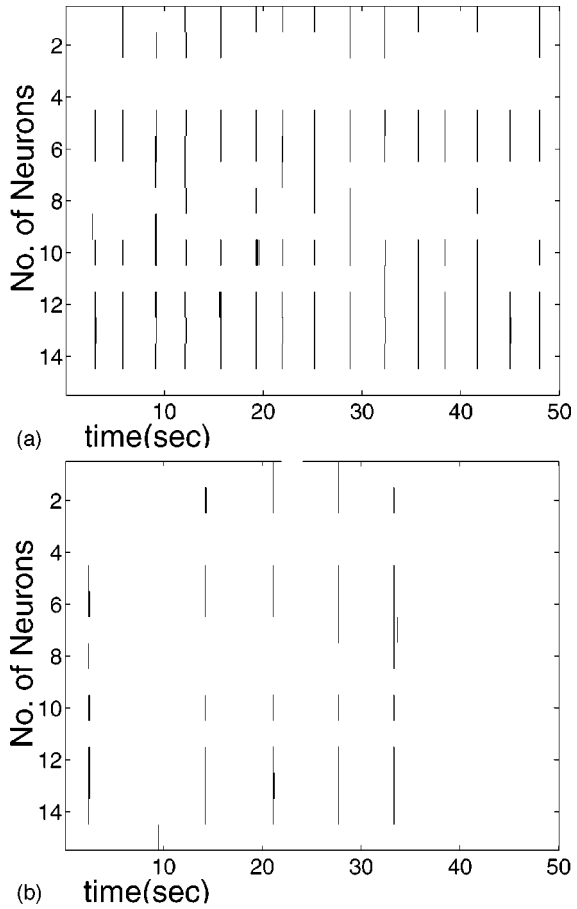

FIG. 6. Network dynamics under 1 mM Ca^{2+} concentration. (a) 1 min after the 1 mM Ca was added. (b) 60 min after the 1 mM Ca was added. At the early time the network shows the almost periodic and rapid (~2 sec) synchronized bursting. However, after 60 min the network activity become aperiodic synchronized bursting. Typically there were 1–6 spikes per neuron for each synchronized event.

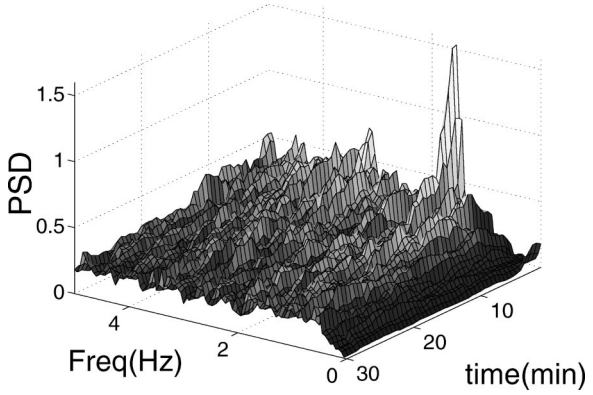

FIG. 7. Power spectral density vs time of network activity under 1 mM Ca concentration. The two high peaks in the PSD correspond to the first and the second harmonics of the activity period. After ~15 min the high periodic activity fades away.

IV. FEEDBACK REGULATED INTEGRATE AND FIRE MODEL

A. Beyond the integrate and fire model

As our starting point in modeling we used the widely studied integrate and fire model. This model captures two key elements of neuronal activity: passive integration of synaptic inputs in the subthreshold domain and generation of an action potential once the threshold has been exceeded (for a review of the integrate and fire models see [14,21,16,22] for a discussion in synchronization of nonlinear oscillators). In the model, each neuron is represented by a leaky capacitor that integrates inputs from synaptic connections and external stimuli. The time dependence of the capacitor voltage is described by the following equation:

$$C\frac{dV_i}{dt} = -\frac{V_i}{R} + \sum_j \overline{W}_{ji}\delta(t-t_k^j) + I_{ext}, \qquad (1)$$

where V_i is the potential of the ith neuron. C and R are the capacitance and resistance of the neuron. $\overline{W}_{ji}$ are the synaptic efficacy between the jth and ith neuron. t_k^j is the kth spike of the jth neuron. I_{ext} is the external current that feeds into the neuron if it is externally stimulated. Since we are interested in spontaneous activity we set $I_{ext}=0$.

The synaptic coupling of the network is taken to be all to all, since our recoding array corresponds to one activity unit. The synaptic efficacies are randomly selected from a uniform distribution $[0,W_{max}]$ and each ith neuron is either excitatory (i.e., $\overline{W}_{ji}>0$ for all j) or inhibitory (i.e., $\overline{W}_{ji}<0$ for all j). We choose 10% of the cells to be inhibitory.

Each neuron integrates the synaptic input, and once the potential V_i reaches a threshold level V_{th}, an action potential is triggered and the charge that has accumulated on the capacitor is shunted to zero. Following the action potential, the neuron enters a refractory period for τ_{ref} time units. During the refractory period the capacitance is zero and the potential is $V_i \equiv 0$. After τ_{ref} the neuron becomes active again.

The above picture is problematic when spontaneous activity is considered. If we start with all the cells' potential be-

low threshold level, we have no activity. In reality, there are internal mechanisms of spike generation below threshold level. Two biophysiological processes contribute to this mechanism: (1) the random opening of ionic channels can induce an ''avalanche'' of channel openings and finally a spontaneous spike (see [14], Chap. 8 for discussion) and (2) the random release of neurotransmitter vesicles in the synapse can induce random excitatory postsynaptic potentials (EPSP's) which are integrated from several sources to generate spontaneous spikes (see [14], Chap. 4 for discussion).

Here we represent these mechanisms in the model by assigning finite probability of firing below threshold level. The firing probability per unit time r is chosen to depend exponentially on the voltage

$$r=\Omega e^{-(V_i-V_{th})^2/T_{eff}}, \tag{2}$$

where Ω is the attempt frequency and T_{eff} is the effective energy barrier.

Simulations of the above specified integrate and fire model produce synchronized activity as is shown in Fig. 8(a), i.e, aperiodic synchronized activity. However, the ISBI histogram [Fig. 8(b)] differs from the observed one. While the simulated distribution of ISBI is finite at zero, the measured one has a cutoff (absolute refractoriness). This model has to be refined. There are two additional known features that are not included in the model at this stage: (1) the dynamic threshold and (2) activity-dependent synaptic connections. Next we test the effect of inclusion on each of these features.

B. The effect of dynamical threshold

First we test the effect of inclusion of the dynamical threshold on the model. This mechanism could be thought of as representing the overall effect on the cell threshold induced by the activation and inactivation of the ionic channels (see [13,15,14] for discussions on similar mechanisms). In our model the cell's threshold depends on the number of available closed channels. Once a spike is triggered, the closed channels open and generate the spike. During the spike, a fraction of the open channels turn inactive while the rest of the open channels return to the closed state. The channels in the inactive state are not opened by the spike and therefore increase the threshold. Specifically, let V_{th} be the cell's threshold. Then

$$V_{th}=\frac{1}{n_c+n_0}, \tag{3}$$

where n_c is the number of the closed channels and n_0 is a constant. Following a spike, the number of closed channels is reduced as follows:

$$n_c \rightarrow (1-\alpha)n_c\,. \tag{4}$$

Thus the number of inactive channels becomes

$$n_i \rightarrow n_i+\alpha n_c\,, \tag{5}$$

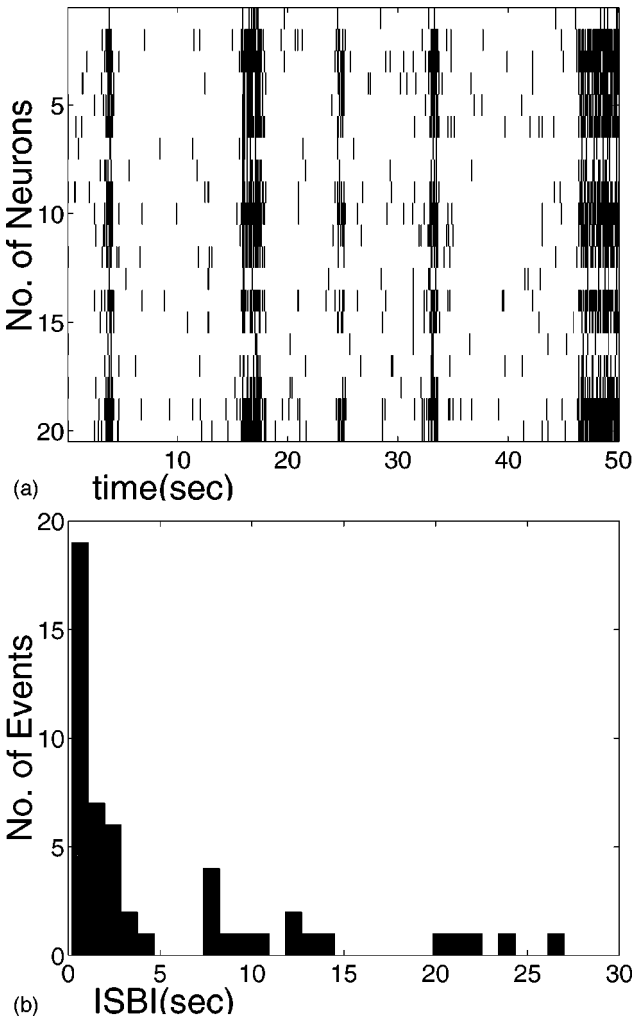

FIG. 8. Simulation of the integrate and fire model. (a) A raster plot of 20 out of 100 cells in the simulation. The neurons fire randomly and from time to time there is a synchronized bursting. (b) histogram of ISBI for the basic integrate and fire model. $RC=10$ msec, $W_{max}=0.36$.

where $0<\alpha<1$ is the fraction of channels that turn inactive. Channels in the inactive state have a finite closing probability per unit time. Thus,

$$\frac{dn_c}{dt}=\frac{n_i}{\tau_{th}} \tag{6}$$

and

$$\frac{dn_i}{dt}=-\frac{n_i}{\tau_{th}}, \tag{7}$$

where τ_{th} is the refractory time constant.

The effect of inclusion of the dynamic threshold is shown in Fig. 9(a). Clearly, the resulting dynamics is in good agreement with the observed experimental data. The neurons fire randomly, and occasionally there are synchronized firing events. Furthermore, the ISBI histogram also agrees with the experimental one as is shown in Fig. 9(b).

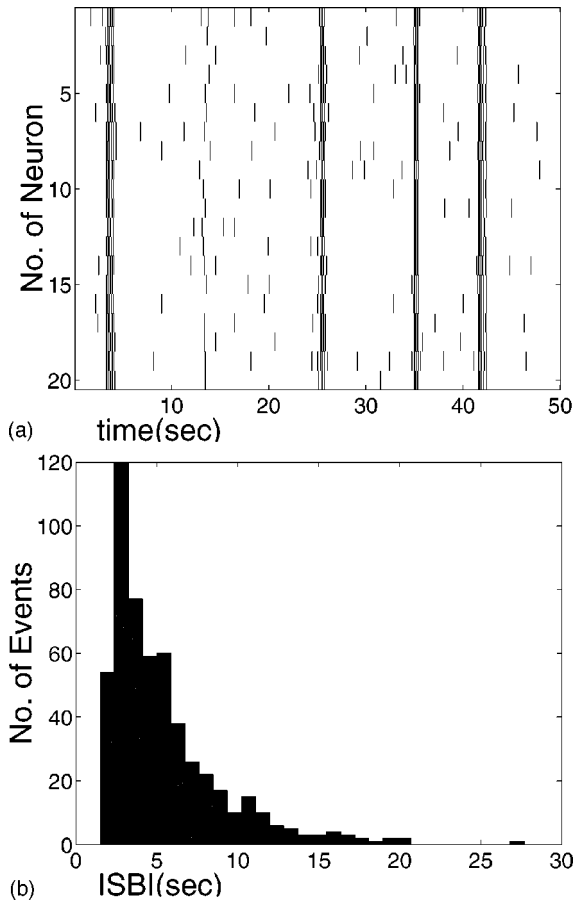

FIG. 9. (a) A raster plot of simulation of network activity when the dynamic threshold is included in the model. The network activity is more regular then before and the $RC=10$ msec, $\tau_{th}=100$ msec, $\alpha=0.4$, $W_{max}=0.1$). (b) A histogram of ISBI for the model with the dynamic threshold.

In order to simulate the effect of Ca concentration we vary W_{max}. In Figs. 10(a), 10(b), and 10(c) we show raster plots of network activity for $W_{max}=0.18$, 0.23, and 0.17, respectively. At the $W_{max}=0.18$ and 0.17 the network activity is aperiodic synchronized bursting as with 0.5 and 2 mM Ca concentrations. When we increase W_{max} to 0.23, the activity becomes fast periodic synchronized bursting as in the case of 1 mM Ca concentrations. Thus, the model can capture the different activity patterns observed experimentally (see Fig. 4).

C. The effect of synapses dynamics

In this section we test the effect of dynamical synapses (see [23] and references therein for a similar mechanism that leads to bursting). There is a known fatigue effect on the synapse strength. During activity the synapse releases the neurotransmitter and reuptakes it during the postspike period. Hence, the synaptic strength is reduced until the amount of neurotransmitter in the synapse is fully recovered. In the model we assign to each synapse a single variable which is the synaptic efficacy W_{ij}. Each time the synapse passes a signal, its efficacy decreases as follows:

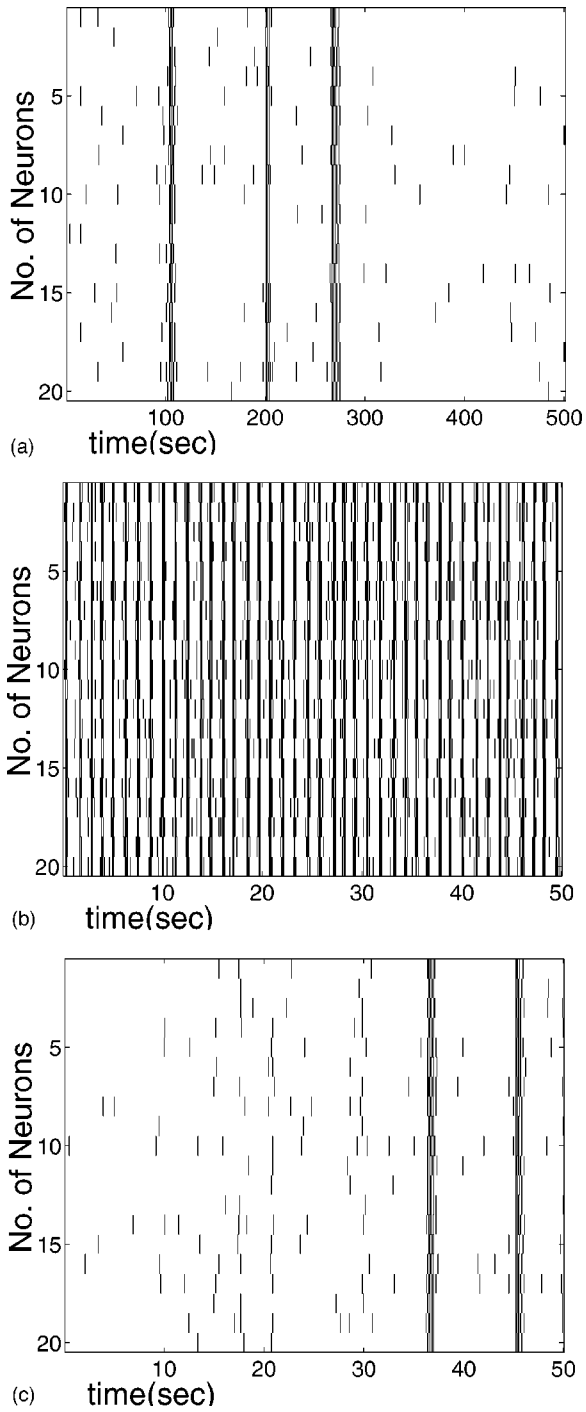

FIG. 10. The fit of the model with a dynamical threshold to the different Ca concentration experiment. In each simulation we adjusted the W_{max} to fit the dynamical state as follows: (a) 0.5 mM Ca, $W_{max}=0.18$. (b) 1 mM Ca, $W_{max}=0.23$. (c) 2 mM Ca, $W_{max}=0.19$.

$$W_{ij}\rightarrow(1-\beta)W_{ij}, \tag{8}$$

where $0<\beta<1$ is a fatigue factor. Between events of neurotransmitter release the synapse efficacy increases continuously

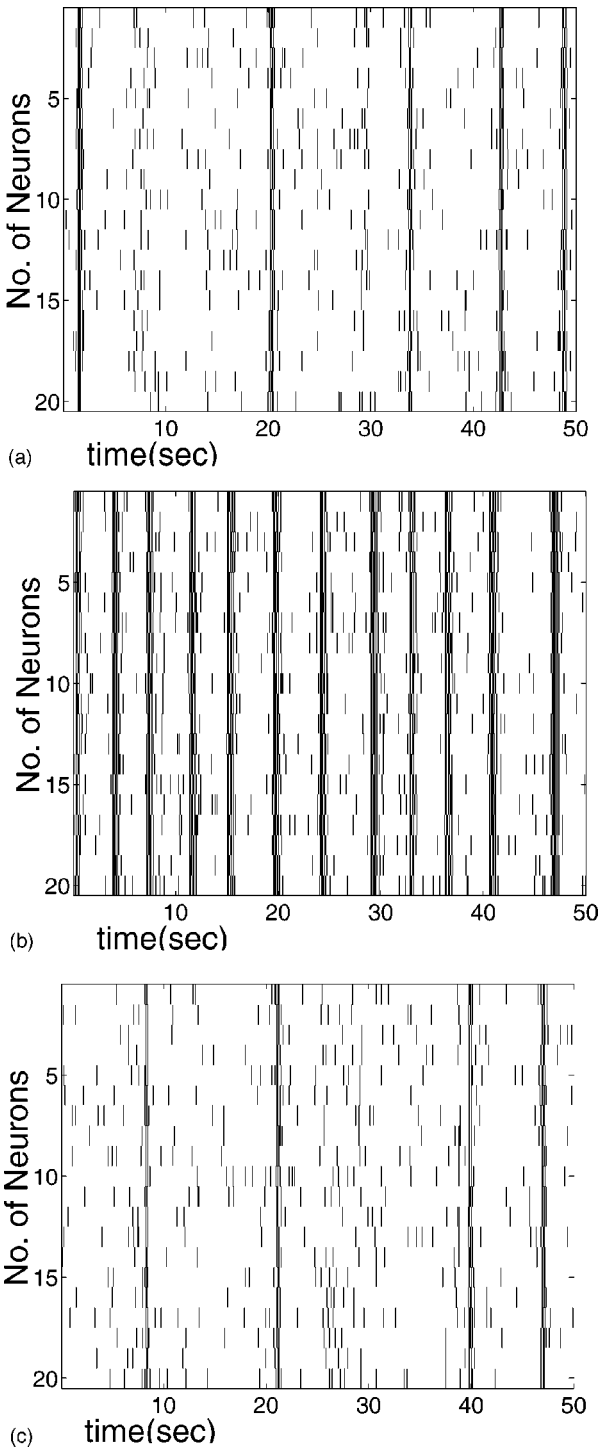

FIG. 11. The fit of the model with dynamical synapses to the different Ca concentration experiment. In each simulation we adjusted the W_{max} to fit the dynamical state as follows: (a) 0.5 mM Ca, $W_{max}=0.275$; (b) 1 mM Ca, $W_{max}=0.6$; (c) 2 mM Ca, $W_{max}=0.28$.

$$\frac{dW_{ij}}{dt} = -\frac{W_{ij}-\overline{W}_{ij}}{\tau_{synapse}}, \tag{9}$$

where $\overline{W}_{ij}$ is the steady-state synaptic efficacy (which is determined randomly as described before). The constant

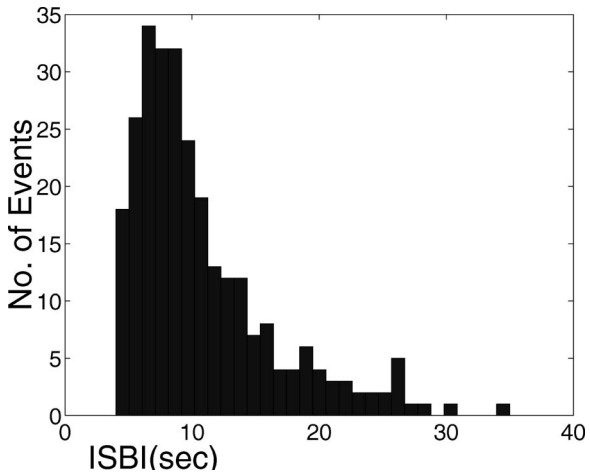

FIG. 12. Histogram of ISBI for the model with dynamic synapses ($W_{max}=0.275$).

$\tau_{synapse}$ is the efficacy-recovering time constant. The effect of the dynamical synaptic strength is shown in Fig. 11. We find a good agreement with the experimental observations.

To capture the effect of calcium concentration, we again vary the level of W_{max}. The results are as shown in Fig. 11. Again, by adjusting the single variable W_{max} we get the normal activity (as in the 0.5 mM Ca^{2+} and 2 mM Ca^{2+} experiments) and the rapid synchronized bursting (as in the 1 mM Ca^{2+} concentration experiments). Furthermore, the ISBI histogram is with a good agreement with the experimental one (Fig. 12).

V. DISCUSSION AND CONCLUSIONS

We have used the multielectrode array technique to study the spontaneous activity of cultured 2D neural networks. The single neuron dynamics shows that each neuron has its own characteristic ISI histogram. On the network level, the most dominant features are the synchronized bursting events. In these events, each of the neurons generates at least one spike and usually several spikes during a time window of $\sim$100 msec. The basic features of the network ISBI histogram are similar to those of the single neurons but the time scale is different. Once a synchronized event is triggered, the system enters an absolute refractory period during which there is no synchronized bursting.

In our measurements, we could not detect a particular spatial organization in the activity during the synchronized bursting events. Note that observation of heart cell tissue culture showed particular spatial organization [24]. This brings to mind that neuron culture might also exhibit such activity. Yet, in our experimental system, the maximum delay of the axonal transport of an action potential from one neuron to another is less then 1 msec as compared to 10 msec of the typical time scale of synapse transport. Therefore, the synaptic delay erases the spatial delay, and there should be no effect of the spatial organization of activity. To unravel the spatial organization one should use electrode arrays with larger spacing.

The experimental observations enable us to develop a

feedback-regulated integrate and fire model. In this model each neuron is represented by a capacitor that integrates the synaptic inputs and generates an action potential when threshold is exceeded. The following two additional features are included: (1) dynamic threshold and (2) activity-dependent synaptic connections. Each of these features can retain most of the observed network activity, from aperiodic activity in the presence of a growth medium to periodic activity in the presence of 1 mM Ca concentration.

Under 1 mM Ca concentration, the network exhibits a transition between periodic and aperiodic activity. Shortly after 1 mM Ca^{2+} is added, the network exhibits almost periodic synchronized bursting which fades away after ~ 20 min. This brings to mind the possibility that the network is adapting to the new conditions. According to this notion, each neuron adapts its synapses or threshold to maintain a level of network electrical activity [25]. The possibility of network adaptation should be verified in experiments of very-long-term ($\sim$days) measurements of spontaneous activity. The transition between periodic to aperiodic activity needs an additional explanation that we did not include in our model at this stage. We hope that additional experimental studies will reveal the relevant information.

ACKNOWLEDGMENTS

We have greatly benefited from conversations with S. Marom and I. Golding. This research has been partially supported by a grant from the Israeli Academy of Sciences, the Sackler Institute for condensed matter physics, the Adams Super Center for Brain Studies, the Kodesh Institute for Medical Engineering, and The Tel Aviv University office for research.

[1] H. Golan, K. Mikenberg, V. Greenberger, and M. Segal, Neural Plasticity **7**, 31 (2000).
[2] G. J. A. Ramakers, J. vanPelt, W. P. M. Willems, W. P. L. C. Rutten, and M. A. Corner (unpublished).
[3] B. C. Wheeler and G. J. Brewer, in *Enabling Technologies for Cultured Neuronal Networks*, edited by D. A. Stenger and T. M. McKenna (Academic, New York, 1994), p. 167.
[4] H. P. C. Robinson, M. Kawahara, Y. Jimbo, K. Torimitsu, Y. Kuroda, and A. Kawana, J. Neurophysiol. **70**, 1606 (1993).
[5] M. Meister, R. Wong, D. A. Baylor, and C. J. Shatz, Science **252**, 939 (1991).
[6] M. J. Gutnick, B. W. Connors, and D. A. Prince, J. Neurophysiol. **48**, 1321 (1982).
[7] A. K. Engel, P. Konig, A. K. Kreiter, T. B. Schillen, and W. Singer, Trends Neurosci. **15**, 218 (1992).
[8] Y. Jimbo, H. P. C. Robinson, and A. Kawana, IEEE Trans. Biomed. Eng. **40**, 804 (1993).
[9] M. Camepari, M. Bove, E. Maede, M. Cappello, and A. Kawana, Biol. Cybern. **77**, 153 (1997).
[10] H. Kamioka, E. Maeda, Y. Jimbo, H. P. C. Robinson, and A. Kawana, Neurosci. Lett. **206**, 109 (1996).
[11] Y. Jimbo, A. Kawana, P. Parodi, and V. Torre, Biol. Cybern. **83**, 1 (2000).
[12] M. O. Maher, J. Pine, J. Wright, and Y. C. Tai, J. Neurosci. Methods **87**, 54 (1999).
[13] Y. Soen and E. Braun, Phys. Rev. E **61**, R2216 (1999).
[14] C. Koch, *Biophysics of Computation* (Oxford University Press, New York, 1999).
[15] I. Opher and D. Horn, Neurocomputing **32**, 161 (2000).
[16] L. F. Abbott and T. Kepler, *Statistical Mechanics of Neural Networks* (Springer-Verlag, Berlin, 1990), pp. 5–18.
[17] I. B. Levitan and L. K. Kaczmarek, *The Neuron* (Oxford University Press, New York, 1991).
[18] U. Egert, B. Schlosshauer, S. Fennrich, W. Nisch, M. Fejtl, T. Knott, T. Muller, and H. Hammerle, Brain Res. **2**, 229 (1998).
[19] E. Hulata, R. Segev, Y. Shapira, M. Benveniste, and E. Ben-Jacob, Phys. Rev. Lett. **85**, 4637 (2000).
[20] P. D. Welch, IEEE Trans. Audio Electroacoust. **AU-15**, 70 (1967).
[21] *Pulsed Neural Networks*, edited by W. Maass and C. B. Bishop (MIT, Cambridge, MA, 1999).
[22] P. C. Matthews, R. E. Mirollo, and S. H. Strogatz, Physica D **52**, 293 (1991).
[23] M. Tsodyks, K. Pawelzik, and H. Markram, Neural Comput. **10**, 821 (1998).
[24] G. Bub, L. Glass, and A. Shrier, Proc. Natl. Acad. Sci. U.S.A. **95**, 10 283 (1998).
[25] J. van Pel, A. van Ooyen, and M. A. Corner, Prog. Brain Res. **108**, 333 (1996).